Supporting Information

Scaled-Down Ionic Liquid-Functionalized Geopolymer Memristors

Maedeh Ahmadipour[1], Mahmudul Alam Shakib[2], Zhaolin Gao[2], Stephen A. Sarles[3, *], Caterina Lamuta[2, *], Reza Montazami[1, 4, *]

[1]Department of Mechanical Engineering, Iowa State University, Ames, Iowa 50011, United States
[2]Department of Mechanical Engineering, College of Engineering, University of Iowa, Iowa City, Iowa 52242, United States
[3]Department of Mechanical, Aerospace, and Biomedical Engineering, University of Tennessee, Knoxville, Tennessee 37916, United States
[4]Department of Agricultural and Biosystems Engineering, Iowa State University, Ames, Iowa 50011, United States

**Corresponding authors. Email: caterina-lamuta@uiowa.edu, ssarles@utk.edu, reza@iastate.edu.*

The diagram in **Figure S1** shows a single channel of the potentiostat used to measure current-voltage characteristics across a geopolymer device.

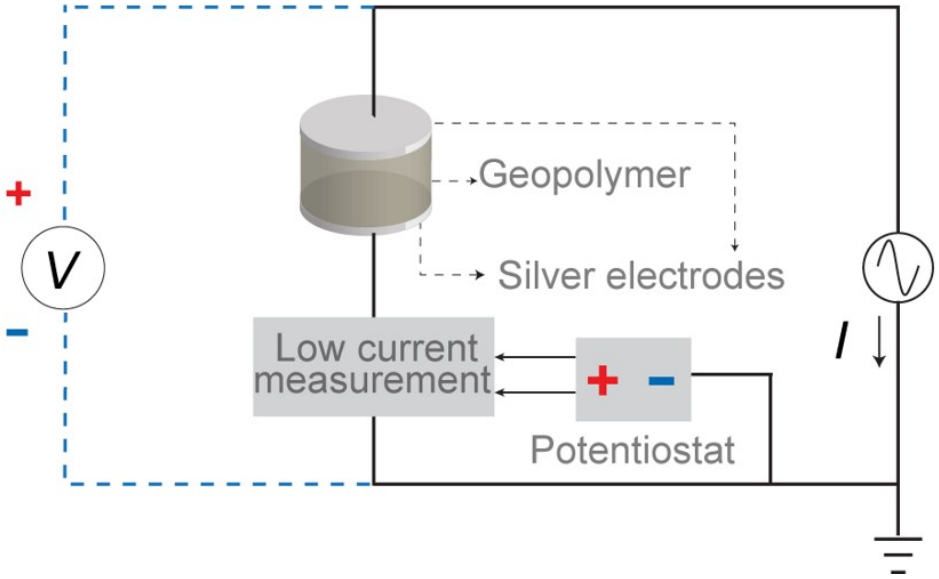

Figure S1. *Circuit diagram showing 2 probes from one channel of the potentiostat were connected to the top and bottom electrode of the device and the current was measured across the geopolymer between the two electrodes for current-voltage characterization. This setup was also utilized for characterization of SRDP, PTP, PPF, and PPD using a single channel of the potentiostat.*

The setup in **Figure S2** shows the potentiostat with two channels used to apply pulses on the top and bottom electrodes of the geopolymer device for spike-timing-dependent plasticity characterization.

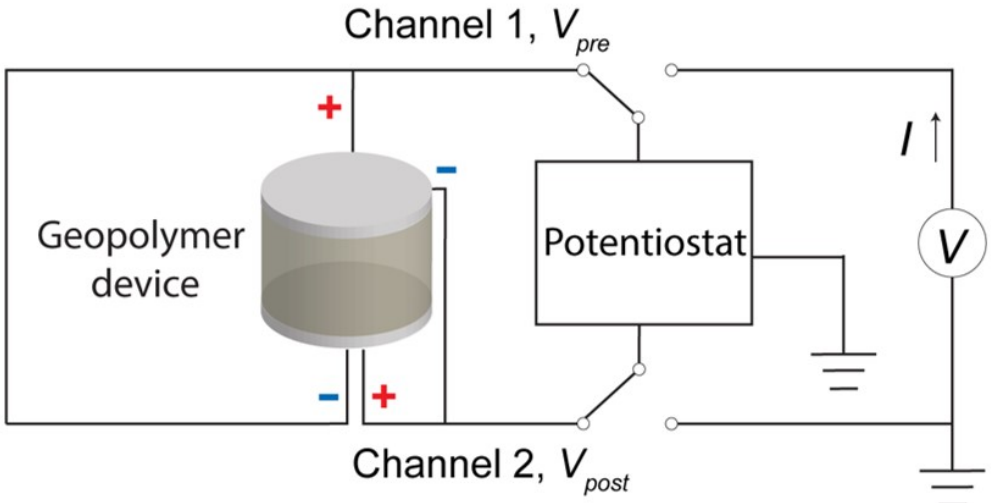

Figure S2. *Circuit diagram showing the test setup for spike-timing-dependent-plasticity (STDP) characterization. 2 channels of the potentiostat were utilized to stimulate the device from top and bottom electrode of the device, respectively, with a pair of pulses.*

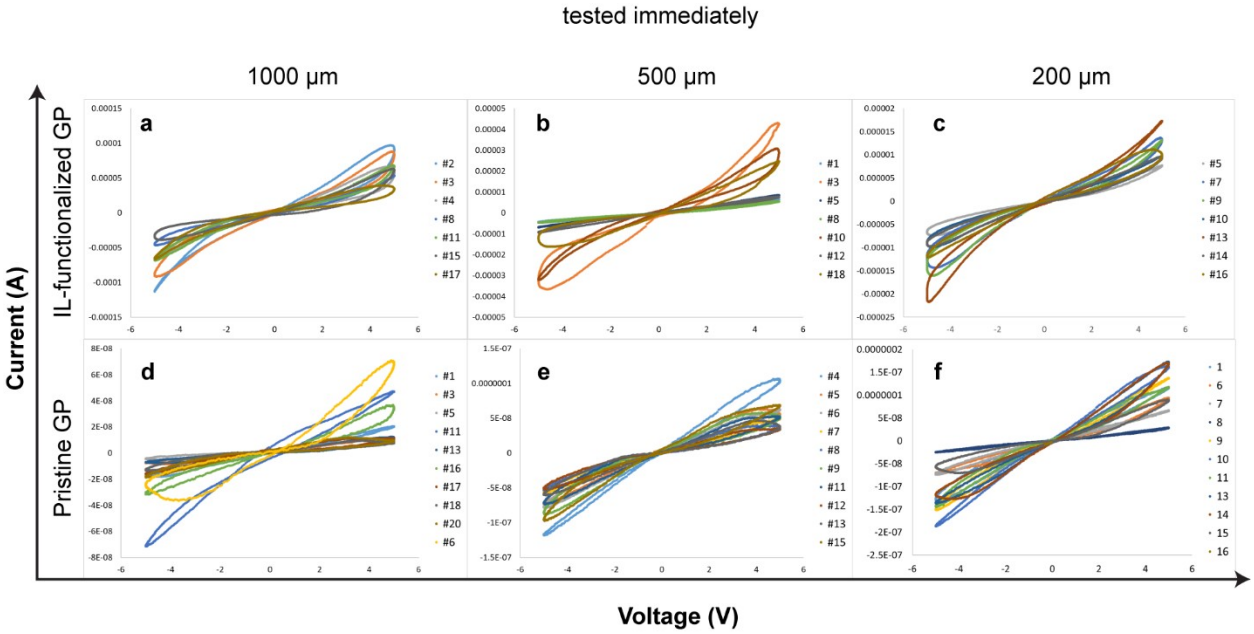

Figure S3. *Comparison of I-V characteristics for IL-functionalized and pristine GP devices with varying dimensions (1000 µm, 500 µm, and 200 µm), tested immediately after fabrication.* ***(a, b, c)*** *Present the I-V curves of IL-functionalized GP devices for three different sizes across seven distinct samples, while* ***(d, e, f)*** *show the I-V curves of pristine GP devices for three different sizes across ten distinct samples.*

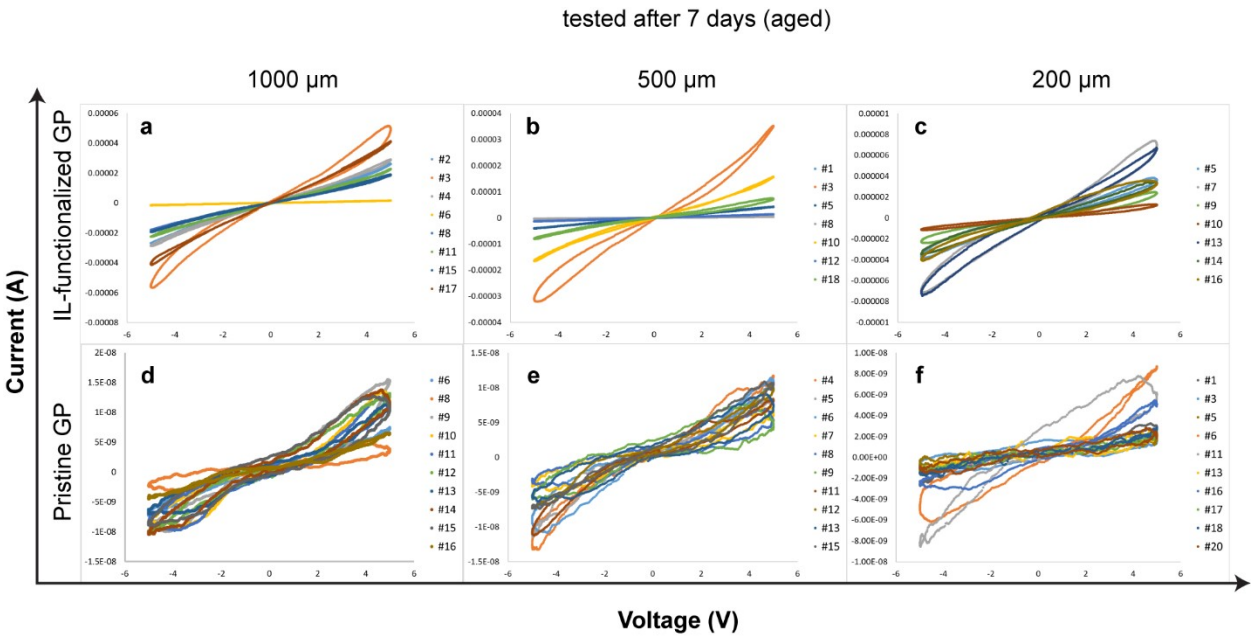

Figure S4. *Comparison of I-V characteristics for IL-functionalized and pristine GP devices with varying dimensions (1000 µm, 500 µm, and 200 µm), tested after one week of aging.* ***(a, b, c)*** *Present the I-V curves of IL-functionalized GP devices for three different sizes across seven distinct samples, while* ***(d, e, f)*** *show the I-V curves of pristine GP devices for three different sizes across ten distinct samples. The IL-functionalized GP devices retained their memristive properties, exhibiting consistent pinched hysteresis behavior even after one week of aging. In contrast, the pristine GP devices largely lost their memristive characteristics, likely due to the evaporation of water within the material. Consequently, many I-V curves for the aged pristine GP samples no longer display the distinct pinched hysteresis behavior.*

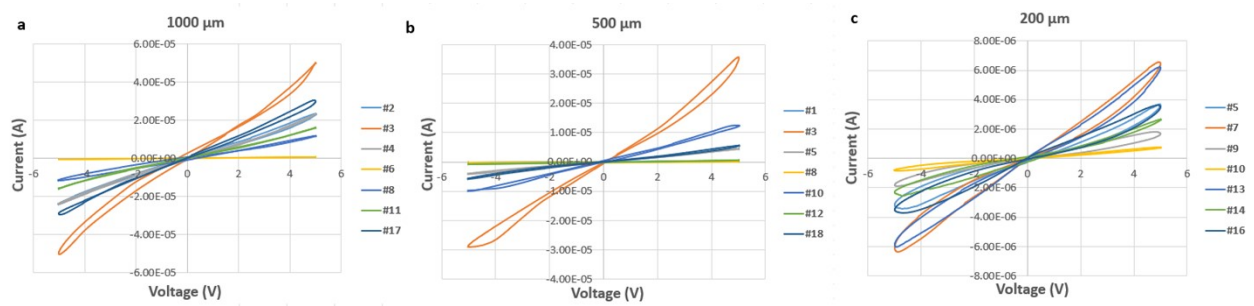

Figure S5. *I-V plots of IL-functionalized geopolymer devices with varying dimensions* ***(a)*** *1000 µm,* ***(b)*** *500 µm, and* ***(c)*** *200 µm, tested after three weeks of aging.*

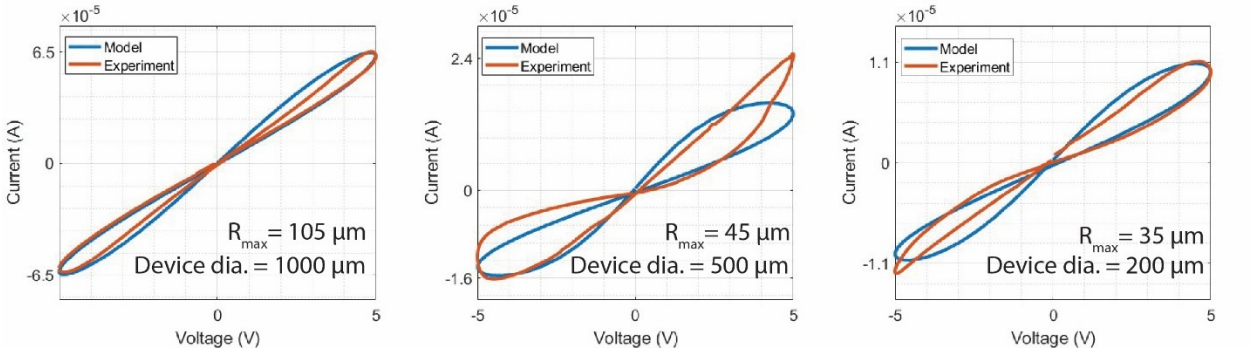

Figure S6. *Comparison of experimental and modeled I-V characteristics for IL-functionalized GP devices with different diameters (1000 µm, 500 µm, and 200 µm) and corresponding maximum pore radius (R_{max}). The experimental data (shown in orange color) and model predictions (shown in blue color) exhibit a decreasing lobe area as R_{max} decreases.*

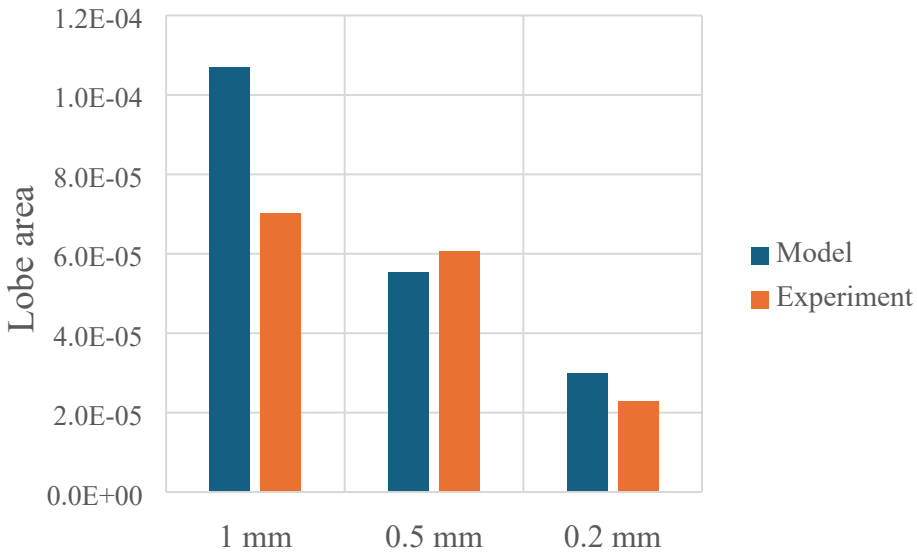

Figure S7. *Comparison of lobe areas from experimental data and model predictions for IL-functionalized GP devices with different diameters.*

Characterization

SEM and EDX

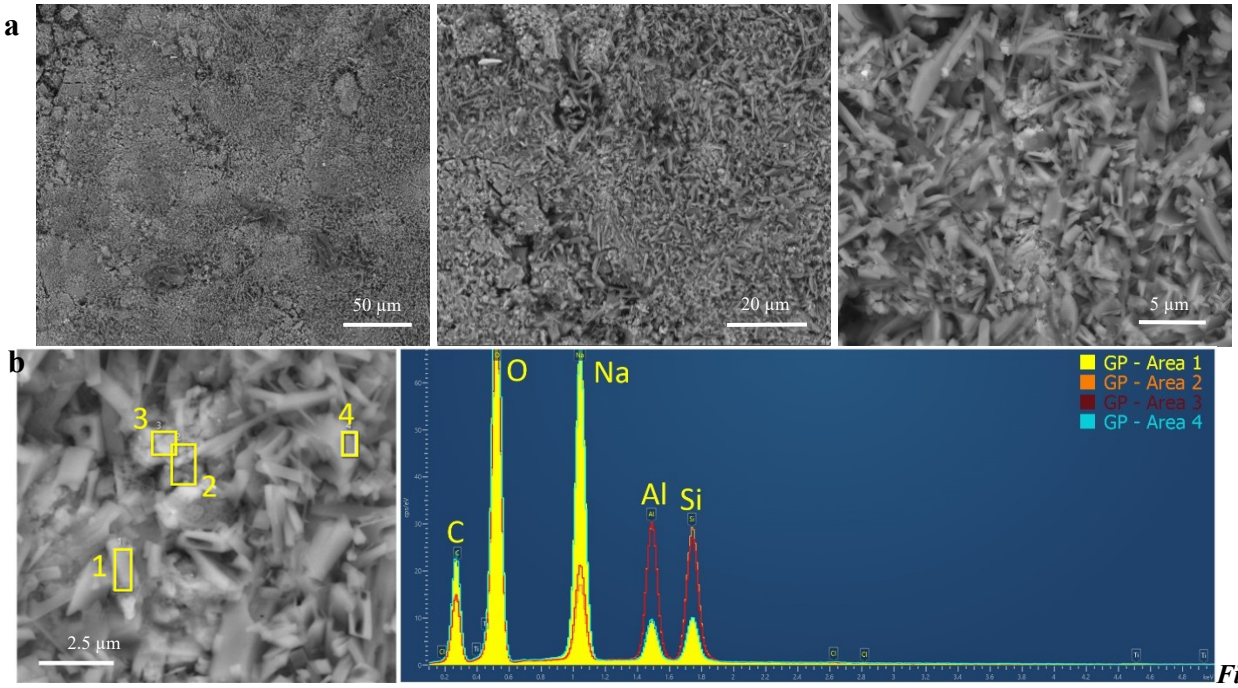

Figure S8. (a) *SEM images of pristine micron-scale GP device;* ***(b)*** *EDX spectra of the same pristine GP.*

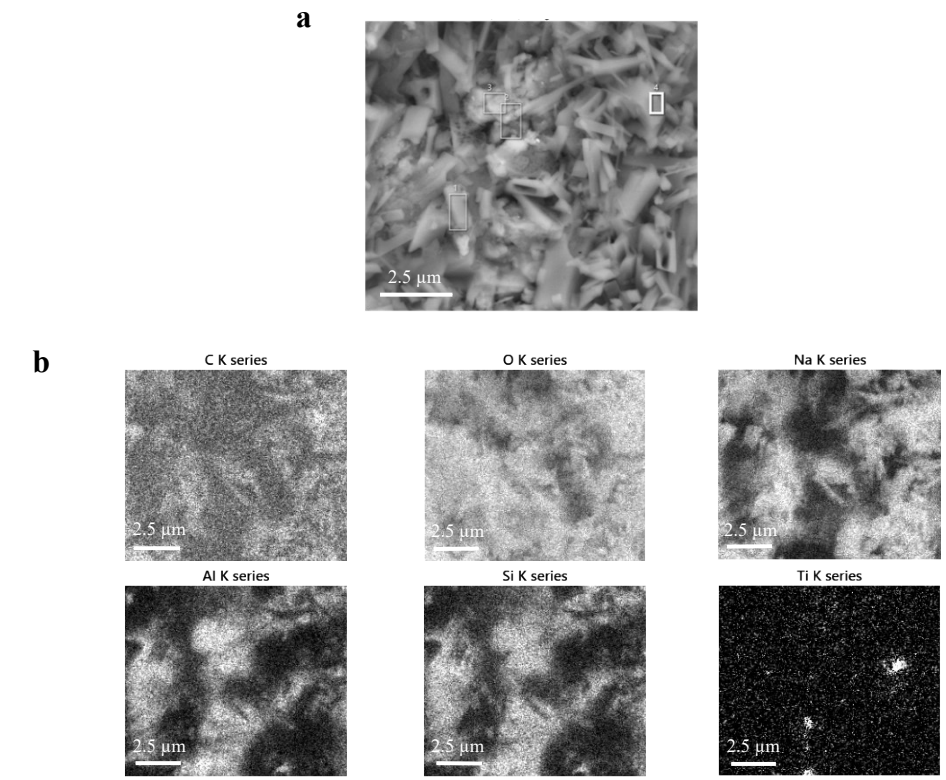

Figure S9. ***(a)*** *SEM image shows the morphology of the pristine GP;* ***(b)*** *The images display EDX elemental maps of the same device, showing all components of the geopolymer including: C and O, both distributed throughout the surface, indicating the organic and oxide components of the geopolymer. Na is present in localized regions, likely from precursor materials. Al and Si are well-distributed, forming the core of the geopolymer matrix, while Ti and Al are attributed to the metakaolin source material, indicating their roles in the structural composition of the geopolymer.*

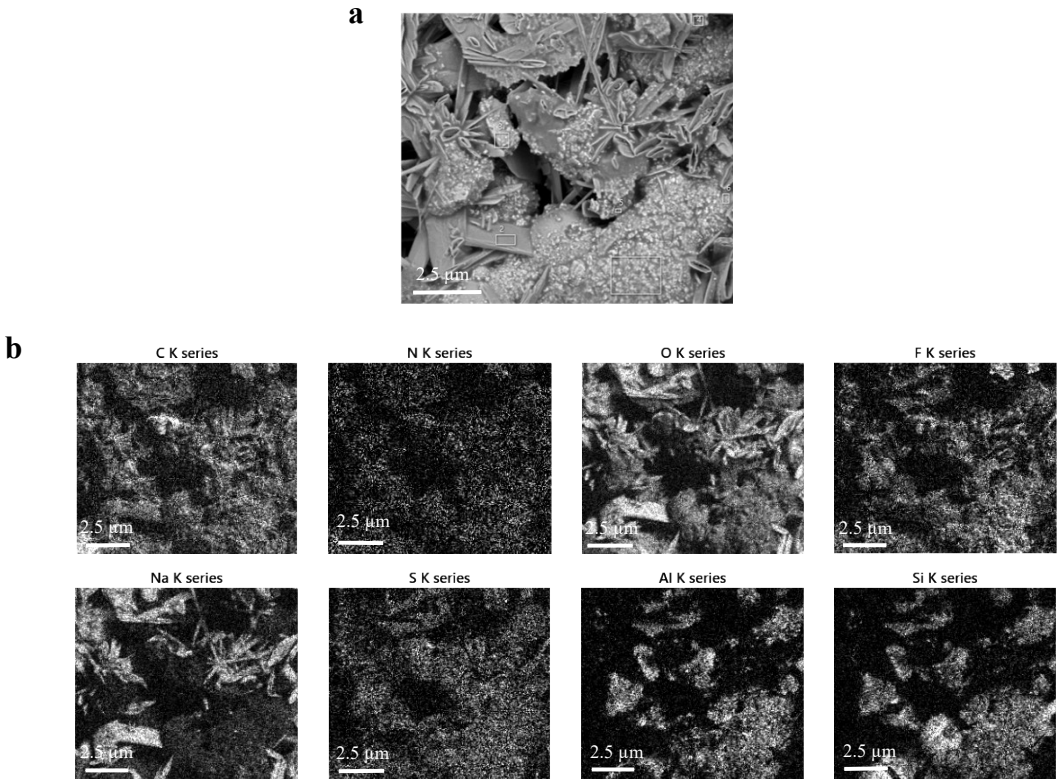

Figure S10. (a) *SEM image shows the morphology of the IL-functionalized GP device before the application of the silver paste layer;* ***(b)*** *The images display EDX elemental maps of the same device, showing the distribution of key elements: C shows homogeneous distribution, indicating good IL integration into the geopolymer. N is more localized, reflecting areas of concentrated IL. S and F, both critical components of the IL, show uneven distributions, suggesting varied IL presence across the surface of the geopolymer device. O, Al, and Si are uniformly distributed, consistent with the geopolymer matrix, while Na appears in distinct regions.*

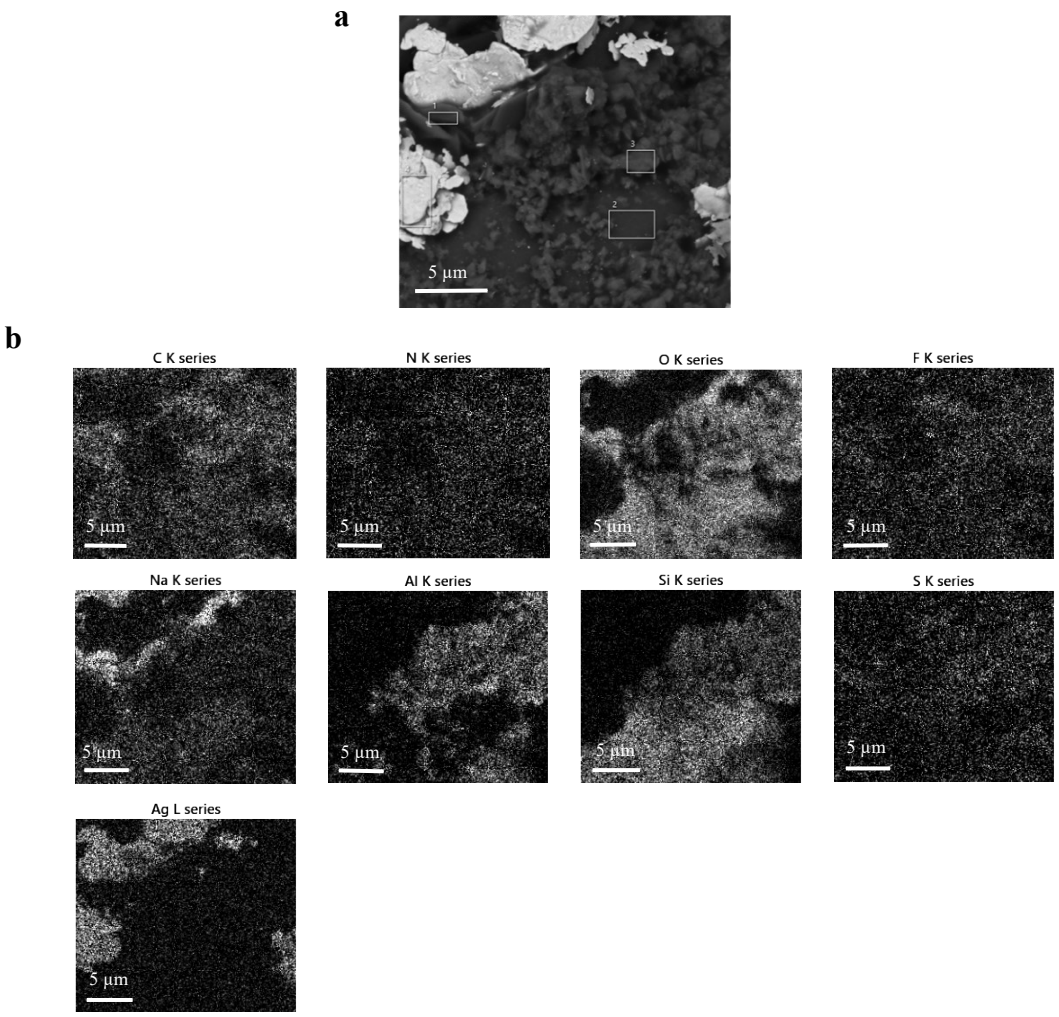

Figure S11. ***(a)*** *SEM image shows the morphology of the IL-functionalized GP device after the application of silver paste layer;* ***(b)*** *The images display EDX elemental maps of the same device, showing the distribution of key elements: C is widely distributed, likely from organic compounds or IL. N is evenly spread, indicating incorporation in the IL. O shows moderate presence, suggesting oxides. F and S appears sparsely, related to IL functionalization. Na is localized in specific regions, likely from residual chemicals. Al clusters indicate its role in the geopolymer, specifically in Metakaolin. Si is uniformly distributed, indicating the silicate framework. Ag is concentrated, marking the silver paste layer application.*

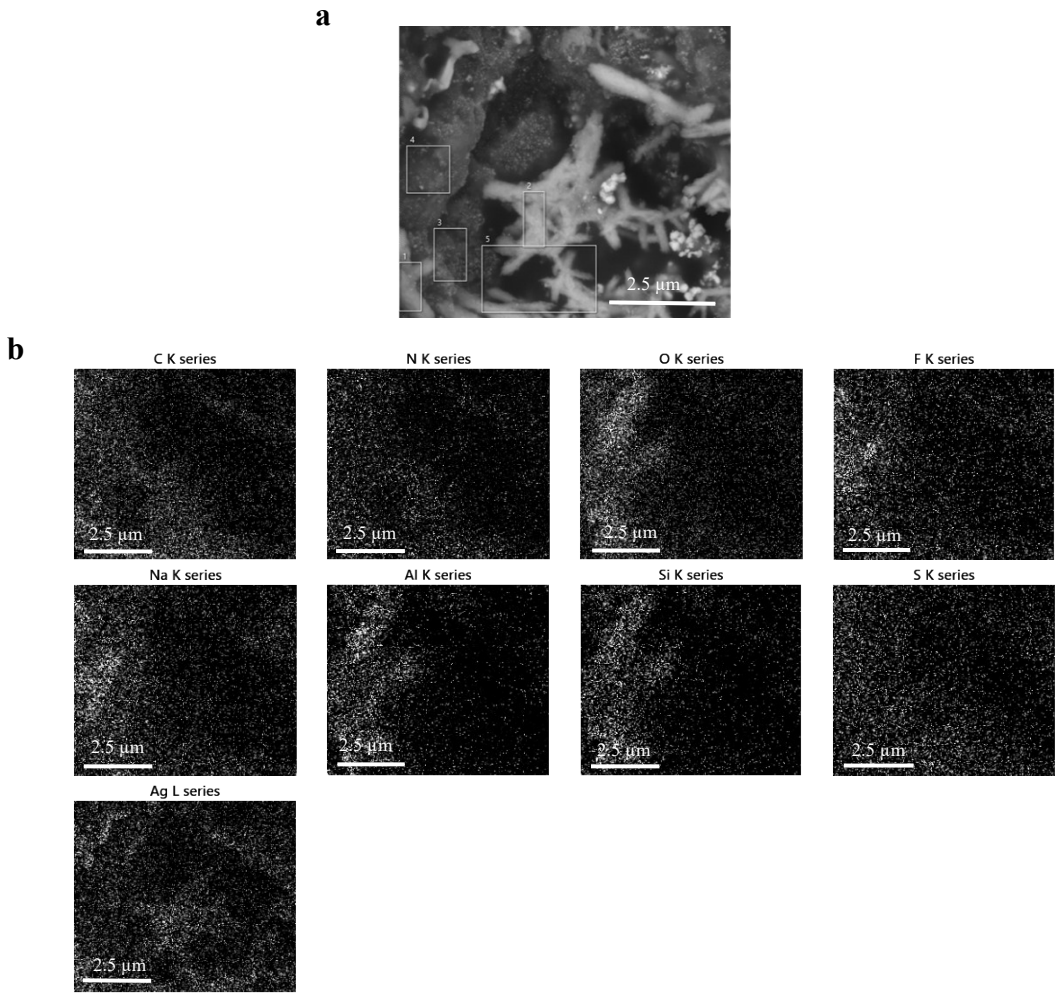

Figure S12. (a) *SEM image shows the morphology of the IL-functionalized GP device after testing under a sinusoidal voltage. Ag metal flakes and also darker crystals of Ag and O are visible, indicating the occurrence of silver oxidation phenomena post-testing;* ***(b)*** *The images display EDX elemental maps of the same device, showing all components of the geopolymer and IL. Specifically, O is widely distributed, playing a significant role in the observed oxidation, particularly around the silver particles and Ag is concentrated in specific areas, with darker regions confirming the oxidation process, aligning with the changes seen in the SEM image.*

ATR-FTIR

The ***Attenuated Total Reflectance Fourier Transform Infrared*** (ATR-FTIR) spectroscopy was performed in the mid-IR range (650 – 4000 cm^{-1}) using a Frontier (Perkin Elmer) ATR-FTIR spectrometer. The ATR-FTIR spectra of the geopolymer samples, as well as the ionic liquid, are presented in **Figure S13**. In **Figure S13a**, the FTIR spectrum of the $EMIM^+$ Otf^- ionic liquid is displayed, while **Figure S13b** shows the spectra for the pristine geopolymer sample both before and after testing. Additionally, **Figure S13c** provides the spectra for the IL-functionalized geopolymer samples before and after testing. Notably, the peaks at 3320 cm^{-1} and 3360 cm^{-1}, characteristic of the $EMIM^+$ Otf^- ionic liquid, are clear in the spectra of the IL-functionalized geopolymer (GP). Furthermore, the fingerprint region reveals prominent C–F and S=O stretching vibrations, which are attributed to the triflate anions of the IL.

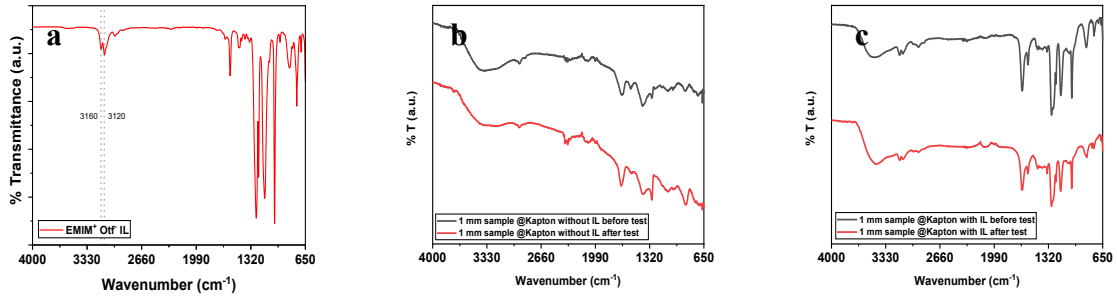

Figure S13. (a) *FTIR spectrum of $EMIM^+$ Otf^- ionic liquid,* ***(b)*** *FTIR spectra of pristine GP sample (D = 1000 µm) before and after test; and* ***(c)*** *ATR-FTIR spectra of IL-functionalized GP sample (D = 1000 µm) before and after test.*

Cyclic voltammetry test results

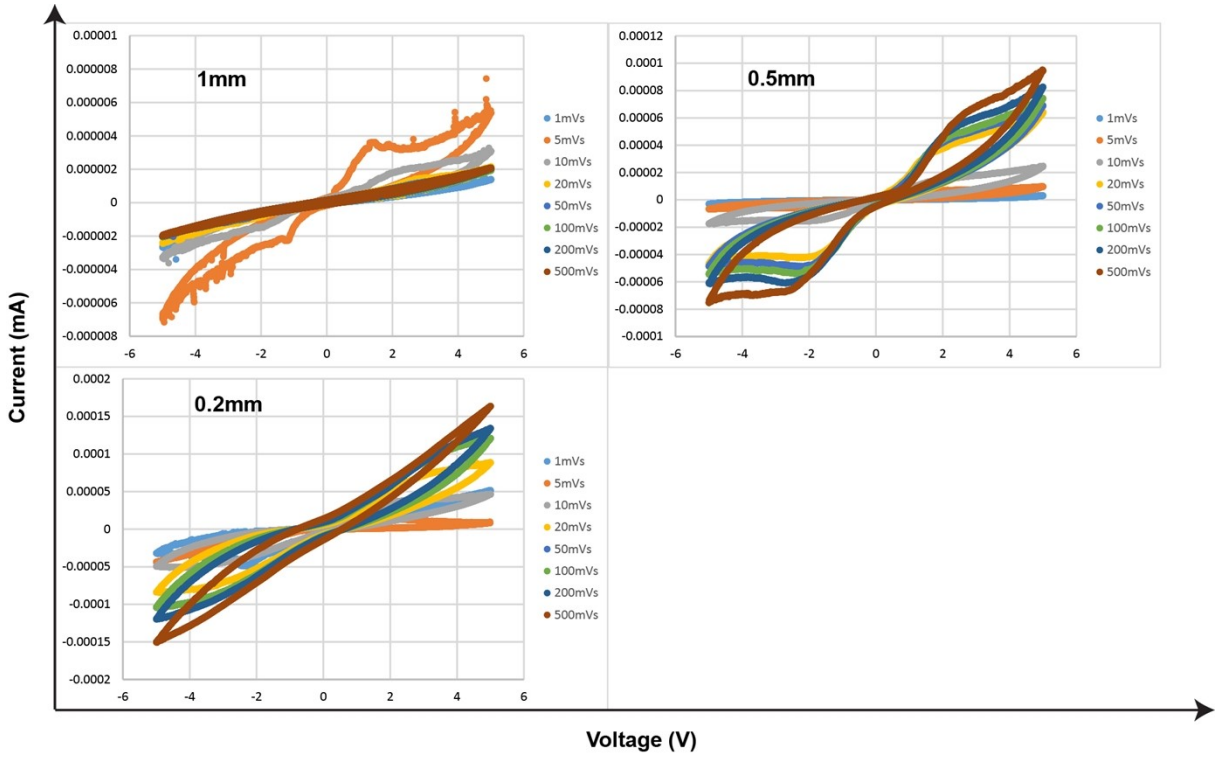

Figure S14. *Cyclic voltammetry plots of pristine geopolymer memristors of sizes 200 µm, 500 µm, and 1000 µm. Tests were repeated for the same samples at different scan rates from 1 mV s^{-1} to 500 mV s^{-1}. The voltage peaks are visible at different scan rates for the same samples.*

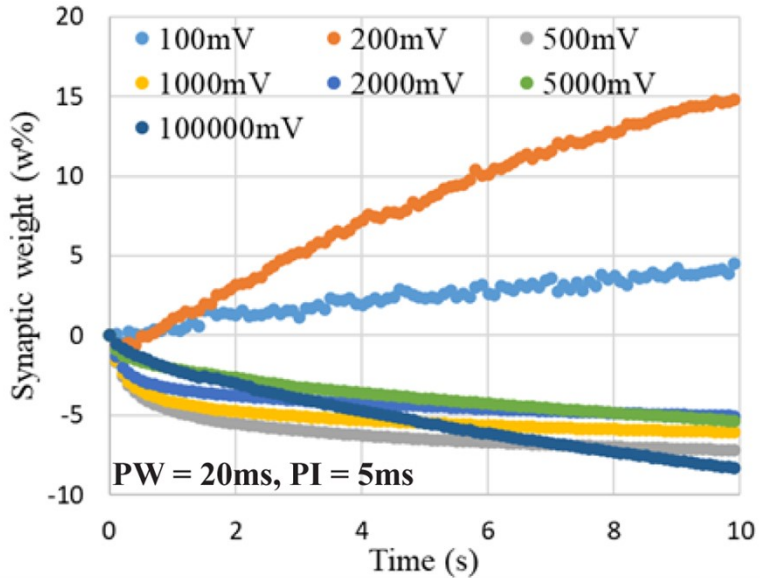

Figure S15. *Pulse train under same pulse width and pulse interval with different pulse heights.*

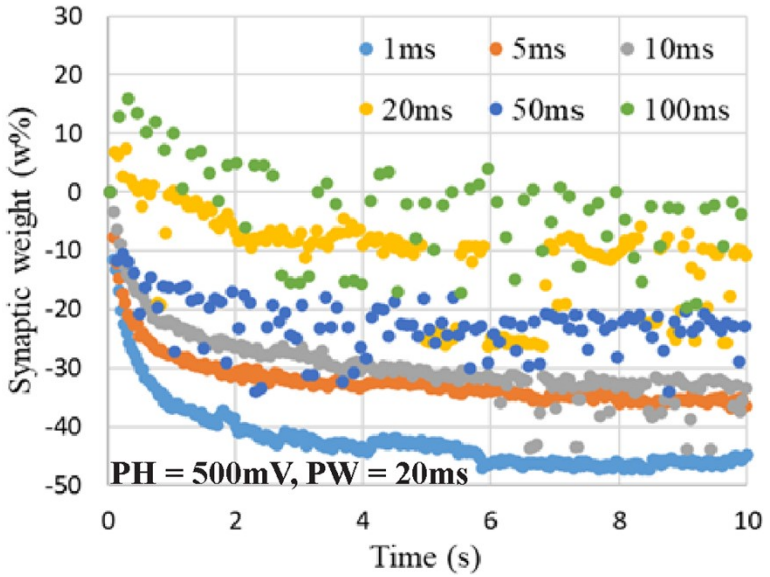

Figure S16. *Pulse train under same pulse height and pulse width with different pulse intervals.*

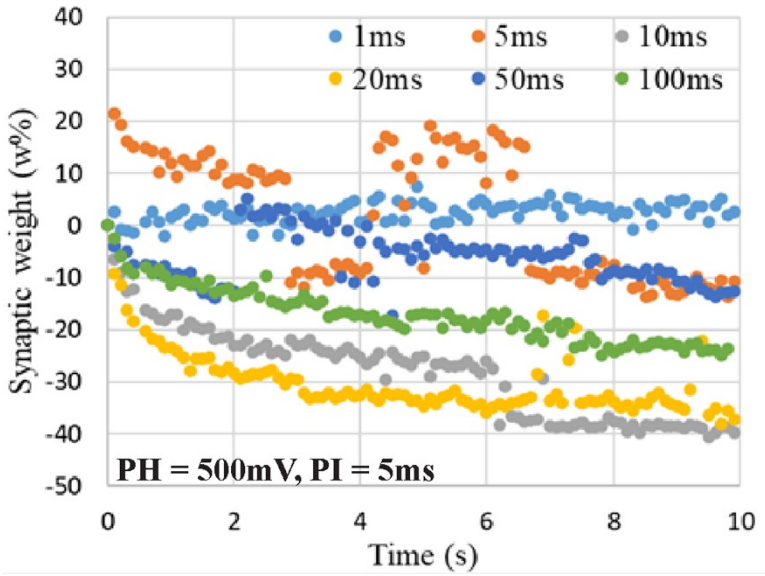

Figure S17. *Pulse train under same pulse height and pulse interval with different pulse widths.*

The result of a paired-pulse facilitation (PPF) test is shown in **Figure S18**, where the current response is represented in red.

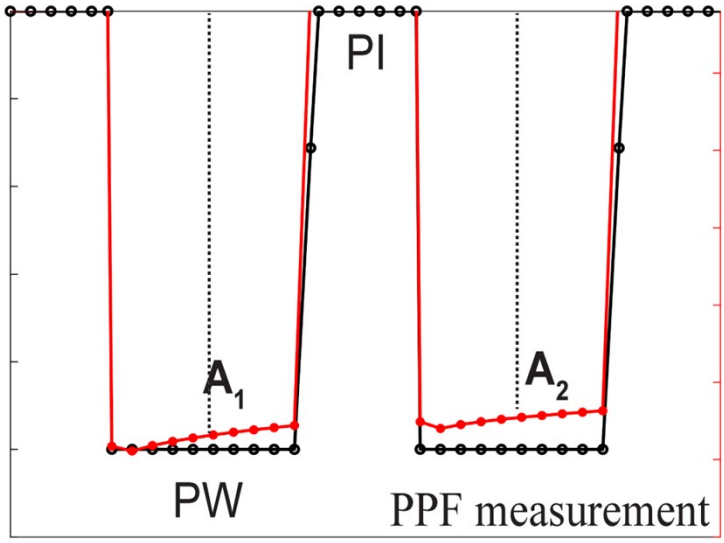

Figure S18. *Shape of the pair of P-spikes and corresponding current signals showing facilitation. Similar pulse pairs were used for PTP, PPF, and PPD demonstrations.*

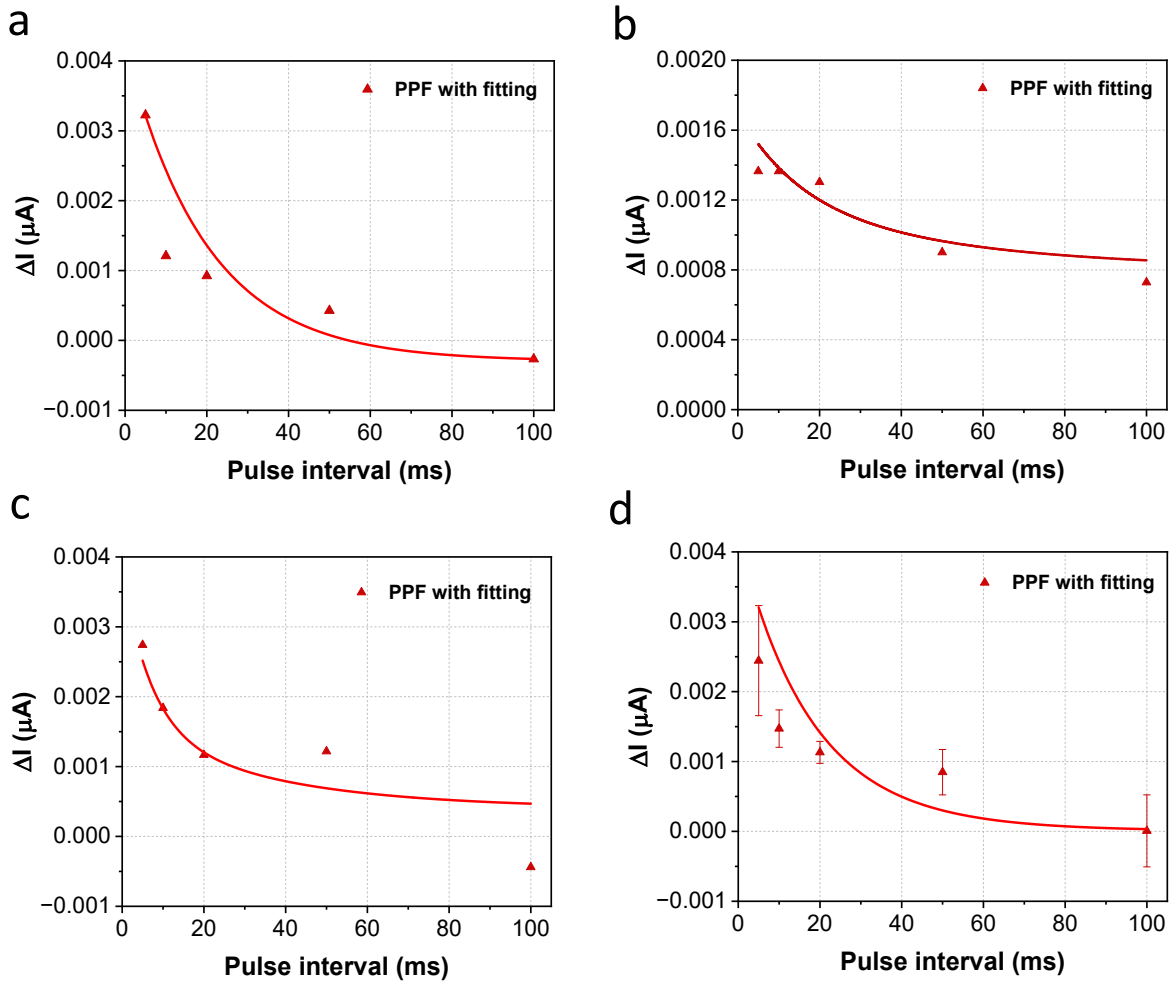

Figure S19. (a-c) *PPF characterization for three individual IL-functionalized geopolymer devices.* ***(d)*** *Average PPF characterization of the three devices shown in (a-c) including corresponding error bars. Data fitting was performed using the equation* $PPF = C_1 e^{-t/\tau_1} + C_2 e^{-t/\tau_2} + C_3$. *The fitted parameters are as follows: for device (a),* $C_1 = 0.00226$, $\tau_1 = 18.033$, $C_2 = 0.00226$, $\tau_2 = 22.040$, $C_3 = -2.980E-04$; *for device (b),* $C_1 = 5E-4$, $\tau_1 = 15$, $C_2 = 4E-4$, $\tau_2 = 50$, $C_3 = 0.0008$; *for device (c),* $C_1 = 0.0022$, $\tau_1 = 7$, $C_2 = 0.0012$, $\tau_2 = 35$, $C_3 = 4E-04$; *and for the average results (d),* $C_1 = 0.00211$, $\tau_1 = 15$, $C_2 = 0.00211$, $\tau_2 = 22$, $C_3 = 7.424E-06$.

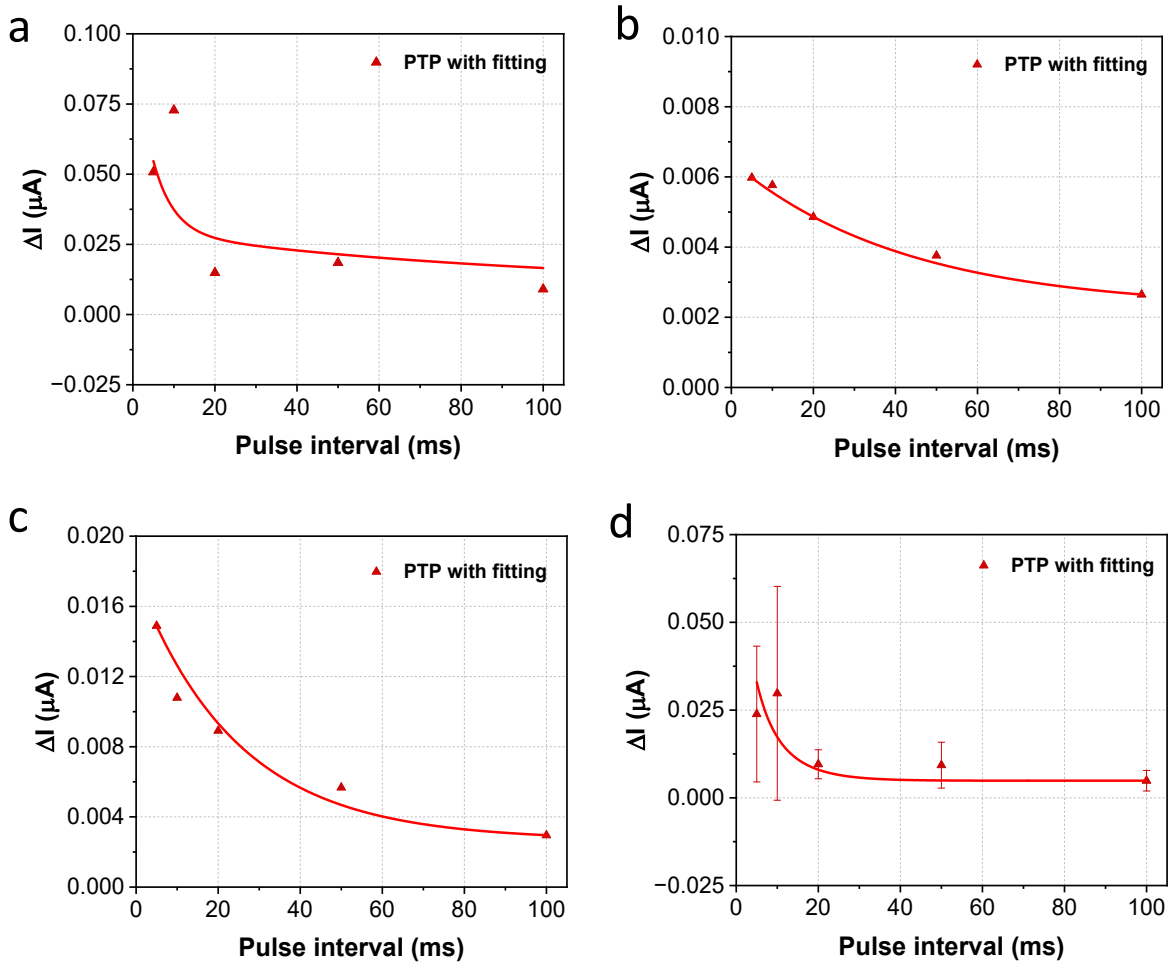

Figure S20. (a-c) *PTP characterization for three individual IL-functionalized geopolymer devices.* ***(d)*** *Average PTP characterization of the three devices shown in (a-c) including corresponding error bars. Data fitting was performed using the equation* $PTP = C_1 e^{-t/\tau_1} + C_2 e^{-t/\tau_2} + C_3$. *The fitted parameters are as follows: for device (a),* $C_1 = 0.07$, $\tau_1 = 5$, $C_2 = 0.02$, $\tau_2 = 90$, $C_3 = 0.01$; *for device (b),* $C_1 = 0.0021$, $\tau_1 = 38.5325$, $C_2 = 0.0021$, $\tau_2 = 47.095$, $C_3 = 0.00224$; *for device (c),* $C_1 = 0.00746$, $\tau_1 = 22.401$, $C_2 = 0.00746$, $\tau_2 = 27.379$, $C_3 = 0.00268$; *and for the average results (d),* $C_1 = 0.03719$, $\tau_1 = 3.296$, $C_2 = 0.03719$, $\tau_2 = 8$, $C_3 = 0.00488$.

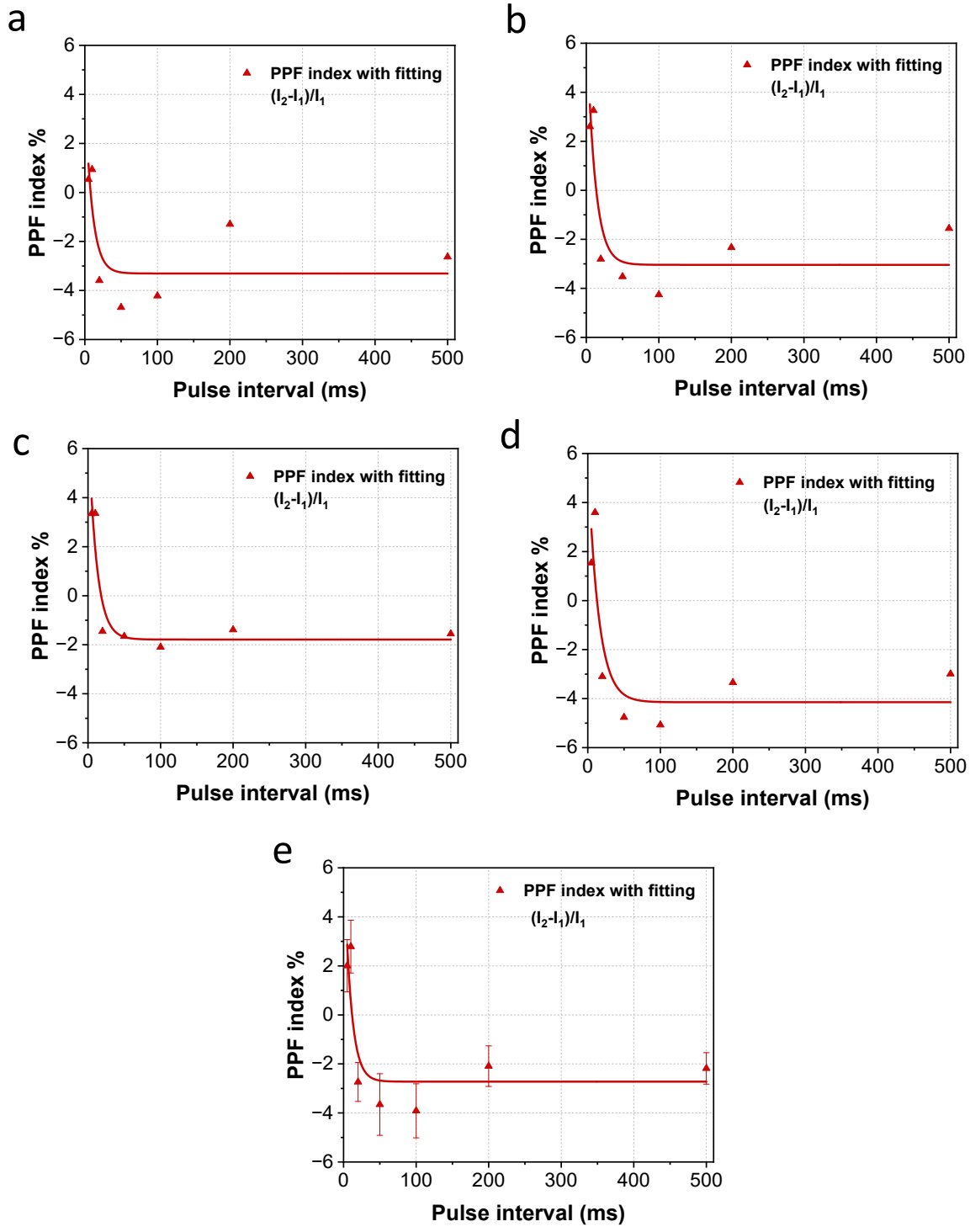

Figure S21. (a-d) *PPF index characterization for four individual IL-functionalized geopolymer devices.* ***(d)*** *Average PPF index characterization of the four devices shown in (a-d) including corresponding error bars. Data fitting was performed using the equation* $PPF\ index = C_1 e^{-t/\tau_1} + C_2 e^{-t/\tau_2} + C_3$. *The fitted parameters are as follows: for device (a),* C_1 *=1.75,* τ_1 *=30 ,* C_2 *=1.75,* τ_2 *=40,* C_3 *=-1; for device (b),* C_1 *=2.27,* τ_1 *=48.71 ,* C_2 *=2.27,* τ_2

=59.53, C_3 *=-10; for device (c),* C_1 *=2.775,* τ_1 *=36.1809 ,* C_2 *=2.775,* τ_2 *=44.22,* C_3 *=-1.9; for device (d),* C_1 *=2.27,* τ_1 *=44.82 ,* C_2 *=2.5,* τ_2 *=54.78,* C_3 *=-10; and for the average results (e),* C_1 *=2.31,* τ_1 *=44.122 ,* C_2 *=2.31,* τ_2 *=53.927,* C_3 *=-2.1819.*